Environmental Science & Technology

Article

pubs.acs.org/est

Characterization of Resistances of a Capacitive Deionization System

Yatian Qu,[†,‡] Theodore F. Baumann,[‡] Juan G. Santiago,[*,†] and Michael Stadermann[*,‡]

[†]Department of Mechanical Engineering, Stanford University Stanford, 440 Escondido Mall, Stanford, California 94305, United States

[‡]Lawrence Livermore National Laboratory, 7000 East Avenue, Livermore, California 94550, United States

Supporting Information

ABSTRACT: Capacitive deionization (CDI) is a promising desalination technology, which operates at low pressure, low temperature, requires little infrastructure, and has the potential to consume less energy for brackish water desalination. However, CDI devices consume significantly more energy than the theoretical thermodynamic minimum, and this is at least partly due to resistive power dissipation. We here report our efforts to characterize electric resistances in a CDI system, with a focus on the resistance associated with the contact between current collectors and porous electrodes. We present an equivalent circuit model to describe resistive components in a CDI cell. We propose measurable figures of merit to characterize cell resistance. We also show that contact pressure between porous electrodes and current collectors can significantly reduce contact resistance. Lastly, we propose and test an alternative electrical contact configuration which uses a pore-filling conductive adhesive (silver epoxy) and achieves significant reductions in contact resistance.

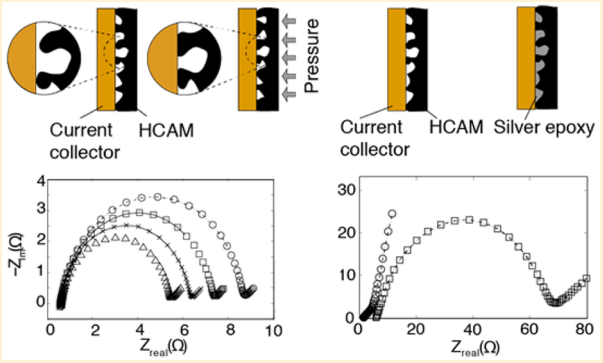

INTRODUCTION

Capacitive deionization (CDI) is an emerging new technique for desalination, with the potential to be cost-effective and energy efficient.[1] It is especially promising for treating water with low and moderate salt concentration, also known as brackish water.[2] CDI operates at low voltage, low pressure and low temperature. It also requires little infrastructure, thus making it scalable to several applications including portable fresh water resource devices, mobile desalination stations for disaster response, and municipal desalination plants.

Most current CDI research focuses on improving salt adsorption capabilities.[1] There are several reported efforts on investigating the actual energy cost of a system[1,3,4] and comparing the thermodynamic efficiency and energy recovery of various operational strategies or modes.[5−7] Energy loss mechanisms in CDI include dissipation through electrical resistances, parasitic redox reactions, and low charge efficiency caused by co-ion repulsion.[8] We know of no studies focused on investigations of CDI resistances as a major contributor of energy loss. The various electrical resistance elements in a CDI cell include the ionic resistance, porous electrode material resistance, current collector resistance, leads, and the contract resistance between current collector and porous electrode. Of course, the instantaneous power dissipated, P_i, by element i of resistance, R_i, is equal to $I_i^2 R_i$, where I_i is the current driven through the element.

The profile of electrical current driven through resistive elements depends on the CDI system's operational mode. Two basic modes, constant voltage (CV), and constant current (CC), have been examined to control energy consumption and charging time.[4,9−11] In the Section S-1 of the Supporting Information (SI), we discuss useful scaling of dissipated power by modeling a CDI system simply and roughly as an RC circuit. R and C are the approximate equivalent resistance and capacitance of the CDI system. We here summarize that discussion as follows. In CV mode, adding resistance proportionally increases charging time (e.g., decreasing overall salt removal rate). Further, half of the energy is dissipated through resistance provided the capacitor is charged for infinite time. However, charging for finite times leads to increased energy dissipation rate, and the dissipated energy depends on resistance. A CC charge mode, by contrast, gives more control over charging rate (hence salt removal rate), and dissipated power is clearly a function of resistance. CC mode can be used to limit initial current (e.g., relative to CV mode) and has been shown to reduce overall energy cost.[11]

Challenges associated with internal resistive losses find similarities across a wide range of electrochemical systems including supercapacitors and batteries. In supercapacitors, methods to reduce system resistances include chemically tuning the pore structure of carbon porous electrodes,[12] using high concentration electrolytes,[13] adding conductive additives such as carbon black,[12] creating contact pressure between porous electrodes and current collectors,[14] increasing pressure and elevating temperature during electrode fabrication[15] and applying surface treatments to current collectors.[16−20] For batteries, commonly used methods for minimizing resistance include thinner electrodes, adjusting active material composition, and improving

Received: February 20, 2015
Revised: July 23, 2015
Accepted: July 27, 2015

DOI: 10.1021/acs.est.5b02542
Environ. Sci. Technol. XXXX, XXX, XXX−XXX

welding structures.[21] Although CDI systems are similar to supercapacitors, CDI resistances have several unique features. In supercapacitors, the electrolyte type and concentration can be chosen to minimize resistance, while in CDI the ionic composition is given by the feedwater. Further, CDI has the goal of reducing ion concentration, and so ionic resistance is nearly always important. Surprisingly, there is currently very limited literature on investigating resistance issues in CDI. Nugrahenny et al. coated ion-selective polymer to the surface of porous electrode to reduce contact resistance.[22] Van Limpt studied the relationship between electrochemical resistance and electrolyte temperature and concentration in a CDI cell.[23] To our knowledge, there is no other published work on resistance characterization of CDI systems. We here focus on a system-wide understanding of resistances in a CDI cell. We present an overview of CDI cell resistance, figures of merit for resistance evaluation, various experimental results on contact resistance, and a proposed new electrical contact configuration. Our study provides methods to both evaluate and address resistance losses in CDI systems.

In this study, we use various experimental methods to characterize major resistive contributors, including four-point measurements, and electrochemical impedance spectroscopy (EIS). As a test case, we characterize and focus on hierarchical carbon aerogel monoliths (HCAMs) electrodes. This material has bimodal pore structures: macropores (0.7−2 μm) which allow liquid transportation with low hydraulic resistance and micropores (sub-10 nm) which provide large surface area (~1500 m^2/g) and high specific capacitance.[24,25] It has been successfully applied to flow-through CDI cell architectures and demonstrated high salt removal and fast responses.[26] Although we here use HCAMs as our model system, our results, recommendations, and figures of merit are applicable to a wide range of CDI designs and electrode types.

OVERVIEW OF CDI CELL RESISTANCE AND DEFINITIONS OF RESISTANCE STANDARDS

Overview of CDI Cell Resistance. Figure 1 shows our proposed simple model to characterize the impedance of a CDI cell. This model has three major components: setup resistance, contact resistance, and the impedance of the porous electrodes (a network of distributed ionic resistance of solution inside electrode, electrical double layer capacitance and electrode bulk material resistance). The total resistance of a CDI cell is then the real component of the total impedance. We here define setup resistance as the ionic resistance of the solution in the separator(s), ionic exclusion membrane (if any) resistance(s), the electrical resistance of current collectors, and resistance of any wires. Contact resistance refers to the interfacial resistance between current collector and porous electrodes. For simplicity, we here treat the porous electrode/ion solution impedance using a classical transmission line. Transmission line (TL) impedance models are commonly applied to simulate electrolyte ionic resistance and capacitance inside the pores of the electrode.[25,27,28] We use a TL model for porous electrodes with bimodal pore structures (with micropores integrated into a macropore network).[25] Figure 1(b) shows the equivalent circuit of a CDI system: R_s, R_{ct}, and Z_{tl} are the setup resistance, contact resistance, and transmission line impedance, respectively. The transmission line impedance includes distributed solution ionic resistances (R_i), electrical double layer (EDL) capacitances (C_i), and the bulk electrical resistances of electrode solid phase (R_e). We assume that macropores determine ionic resistance

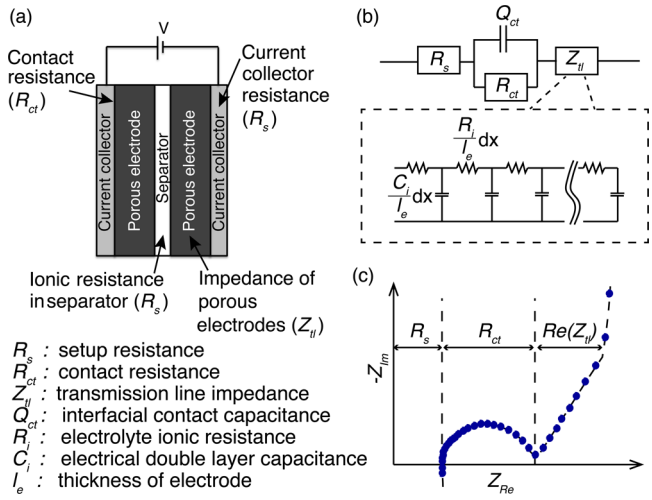

Figure 1. (a) Schematic of total resistance in a CDI cell. We characterize resistive components into three groups: setup resistance R_s, contact resistance R_{ct}, and transmission line impedance Z_{tl}. (b) Corresponding equivalent circuit of a CDI cell. (c) Schematic of a typical Nyquist plot of EIS response of a CDI system. The semiellipse feature is associated with contact resistance and a constant phase element of contact capacitance.

and micropores dominate EDL capacitance.[25] We use a constant phase element Q_{ct} to model the interfacial capacitance of current collectors.[23,29] This nonideal capacitor is in parallel with R_{ct}. We also extract an approximate interfacial capacitance estimate C_{ct} from the best-fit estimate of the constant phase element parameter Q_{ct}.[30] Figure 1(c) shows the schematic of a typical Nyquist plot of electrochemical impedance spectroscopy (EIS) response of a CDI cell. The semiellipse is a typical response of an assembled CDI cell, and this feature is due to the parallel connection of contact resistance and interfacial capacitance of the current collector.[14,15,29,31]

Area Normalization of Resistance, Area-Normalized Equivalent Series Resistance and Area-Normalized Operational Nominal Resistance. Perhaps the most direct way of obtaining contact resistance is from EIS. As indicated in Figure 1(c), setup resistance, contact resistance, and interfacial capacitance can be extracted from the semiellipse feature at high frequencies. The setup resistance is the value of the leftmost intersection of semiellipse feature with axis Z_{Re}. The contact resistance R_{ct}, and constant phase element Q_{ct} are in parallel, and so the major diameter of the semiellipse feature quantifies the contact resistance value R_{ct}, and the frequency associated with the apex of the semiellipse quantifies the constant phase element Q_{ct}, thereby providing an estimate for the interfacial contact capacitance C_{ct}.

Since EIS data are not always available, we here propose two area-normalized resistance metrics that can be measured by simpler means and also extracted from published data: area-normalized equivalent series resistance (ANESR) and area-normalized operational nominal resistance (ANONR). We advocate the use of area-normalized resistances, as it allows the comparison of resistance across device designs. We use ANESR to estimate the importance of contact resistance, and ANONR as a figure of merit to evaluate the cell performance. The ANESR can be estimated from CV or CC charging/discharging profiles and cell geometries. The ANONR is approximately the upper limit of the cell's effective resistance during an entire charging/discharging cycle. We summarize the evaluation

DOI: 10.1021/acs.est.5b02542
Environ. Sci. Technol. XXXX, XXX, XXX−XXX

Table 1. Definition of Our Proposed Cell Resistance Figures of Merit

area-normalized equivalent series resistance[a] (ANESR) [Ω-cm^2] $(R_s + R_{ct})AN$				area-normalized operational nominal resistance[b] (ANONR) [Ω-cm^2]
constant current		constant voltage		
charging	discharging	charging	discharging	
$(\Delta V_{meas}/I_{CC})AN$	$(\Delta V_{meas}/I_{CC})AN$	$(V_{CV}/\Delta I_{meas})AN$	$-(V_{CV}/\Delta I_{meas})AN$	$(R_s + R_{ct} + 1/2R_i)AN$

[a]ANESR is a measured quantity. Subscripts CC and CV in expressions indicate the controlled/fixed parameter. Subscript "meas" indicates the measured values. A is the geometric area (projected in the primary direction of electrical current) for each electrode, and N is the number of cells electrically in parallel in a cell stack. [b]ANONR is a predicted parameter obtained from estimates of R_s, R_{ct}, and R_i. See Section S-6 in SI. A is the geometric area of the electrode, and N is the number of cell electrically in parallel in a cell stack.

equations of these two standards in Table 1 and provide detailed descriptions below.

Area Normalization of Resistance. To compare performance between CDI cell devices and designs, we propose the use of area normalization as a general standard to evaluate each resistance merit:

$$R_{abs}AN \quad (1)$$

Here, R_{abs} is the absolute value of the measured or estimated resistance of interest for the CDI cell. As shown in Table 1, R_{abs} equals $R_s + R_{ct}$ for ANESR and $(R_s + R_{ct} + 1/2R_i)$ for ANONR. We provide example methods to measure or estimate these resistances in the SI. N is the number of (electrically parallel) cells in the stack, and A is the area of each electrode. CDI devices in literature vary widely in length scales (and number of cells in parallel), ranging from a single unit with electrode areas of a few square centimeters to a full stack cell with hundreds of pairs of electrodes with each electrode area as large as a hundred square centimeters. Hence, absolute resistance (in Ohms) is not an appropriate figure of merit. We advocate the use of this area normalization as a standard to describe and compare CDI devices.

Area-Normalized Equivalent Series Resistance. In Table 1, we summarize the equations to obtain ANESR in each of the CC and CV modes. Within each mode, we also describe the equations of ANESR in charging and discharging states. For CC mode, we first determine absolute charging (discharging) equivalent series resistance (ESR) as the instant voltage rise (drop) very shortly after the time when constant current is applied (reversed) divided by the current, as shown in Figure S-2a. For CV operational mode, we obtain the absolute charging (discharging) ESR as the constant voltage divided by the instant charging (discharging) current very shortly after the voltage is applied (removed), as shown in Figure S-2b. As per our model, this ESR is approximately the sum of setup resistance and contact resistance: $R_s + R_{ct}$. We then normalize ESR by electrode geometric area A and cell number in a stack N to obtain ANESR, $(R_s + R_{ct})AN$. See SI for more details.

Area-Normalized Operational Nominal Resistance (ANONR). Our proposed ANONR is based on simulations of our equivalent circuit model which we performed using LTSpice (Linear Technology Corporation, Milpitas, CA). We used these to investigate current or voltage responses of a CDI cell in both CC and CV operation modes. These simulations suggest that the input current of a CDI cell in operation is approximately evenly distributed between bulk electrode resistance, R_e, and the solution ionic resistance R_i in the porous electrode (within the TL network, see SI section S-6). Therefore, we can estimate the effective resistance of the TL network of electrodes as $(R_i + R_e)/2$ during operation. Further, since R_e is everywhere in parallel with the resistance of the ionic solution, and R_e is negligible compared to R_i, the TL network resistance $(R_i + R_e)/2$ can be approximated as $R_i/2$. We then estimate the absolute resistance of a cell in operation as the sum of setup resistance, contact resistance and half of the solution ionic resistance in porous electrodes: $R_s + R_{ct} + R_i/2$. We then normalize this absolute operational nominal resistance by electrode geometric area A and cell number in a stack N to obtain ANONR, $(R_s + R_{ct} + R_i/2)AN$. The value of ANONR is important as it sets the approximate upper limit of the cell's resistance during a complete operation cycle. However, in both CV and CC mode, this resistance is difficult to measure experimentally, due to the challenge of accurately estimating the solution ionic resistance inside electrodes R_i from charging/discharging profiles. We also note that the ionic resistance R_i of a CDI cell is in fact time dependent and, of course, a function of the distributed network structure of resistances and capacitances of the electrode. We here use a nominal value of R_i to approximate the ionic resistance inside porous electrodes. R_i is estimated by modeling the porous electrodes as a large number of idealized and tortuous microchannels in parallel[32] (see SI section S-2). Our proposed R_i can be interpreted as the net value of ionic resistance of the solution inside the entire electrodes in the absence of charging or discharging of its capacitance elements.

MATERIALS AND METHODS

Ex Situ Measurement of Contact Resistance Using a Custom Four-Point Probe. We designed a custom resistance measurement platform to characterize the ex situ contact resistance between a single porous electrode and a single metal current collector (Figure 2a). This measurement is a modification of standard four-point test. A 2.5 × 2.5 × 0.24 cm^3 copper plate was in facial contact with a 2 × 2 × 0.22 cm^3 HCAM piece. The actual contact area was 2 × 1.7 cm^2. Two wires were connected to the largest face of copper plate via silver epoxy with one connection in the middle, a second near the edge. The distance between the two wires was 10 mm. The HCAM piece was in contact with a custom-designed printed circuit board (PCB) (Sunstone Circuits, Mulino, OR). This PCB was designed to create two electrical contact points with the HCAM material for four-point probe tests. The PCB included two round silver-coated contact pads 1.5 mm in diameter and with an intervening gap of 10 mm. The copper plate, HCAM piece, and PCB board were assembled and placed into an acrylic housing to accurately control the overlap area between copper plate and HCAM piece. As shown in Figure 2a, the assembled experiment used a copper plate and a PCB on each side of the porous electrode layer to achieve a four-point probe measurement. Current was forced through node A on copper plate, driven through the interface between copper plate and HCAM piece, then exited at node D from PCB board. A voltage

DOI: 10.1021/acs.est.5b02542
Environ. Sci. Technol. XXXX, XXX, XXX−XXX

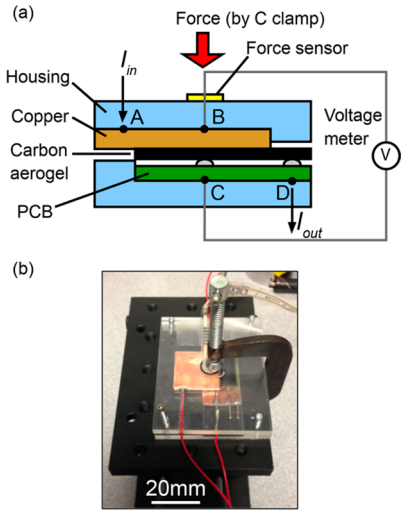

Figure 2. (a) Experimental setup and (b) image of custom four-point (points A–D) measurement platform for ex situ characterization of contact resistance. We used a PCB board to facilitate the four-probe measurement. The PCB board, a copper plate, and a HCAM sample were aligned and held by acrylic housing and a C-clamp. The C-clamp applied external force perpendicular to the platform to compress HCAM sample against current collector. The force was monitored through a force sensor interfaced with a DAQ card.

difference resulting from this known current was measured between the inner two nodes B and C with a DAQ card (NI USB-6009, National Instruments, Austin, TX). This voltage difference was nearly perfectly dominated by the contact resistance at the interface. A force sensor was mounted onto the surface of upper housing piece in the middle. We used a C clamp to apply force to the device and the force is monitored through the force sensor. Figure 2b shows an image of the assembled experiment set up. We performed these experiments with dry HCAM samples to exclude the influence of ionic resistance and interfacial capacitance.

CDI Cell Assembly with Standard Current Collectors for in Situ Resistance Measurement. We fabricated a flow-through CDI cell design using two blocks of HCAM material with dimensions of 2 × 2 × 0.1 cm^3 for in situ resistance characterization. We used titanium plates as current collectors in the cell and a porous polypropylene separator (Celgard 3501, Charlotte, NC) to insulate between the two electrodes. The porous electrodes, separator, and current collectors were held together as an assembly using heat shrink tubing. The housing parts were fabricated from polycarbonate by CNC machining. The cell was designed to apply a known compression stress to the assembly by tightening two 5–40 screw fitted on each side of its frame.

Electrochemical Impedance Measurements of an Assembled CDI Cell. The resistance of the entire CDI cell was characterized by EIS using BioLogic SP-300 potentiostat (Bio Logic Science Claix, France). EIS was performed in a two-terminal configuration without a reference electrode since the electrodes of the cell were symmetric. We applied a 10 mV amplitude sinusoidal potential perturbation and scanned over a frequency range from 2 MHz to 10 mHz at 0 V bias. During electrochemical tests, the cell was filled with either 2 M NaCl or 100 mM NaCl. We waited 30 min before performing EIS measurements to allow the cell to equilibrate with the sodium chloride solution.

RESULTS AND DISCUSSION

Diagnosis of CDI Cell Resistances. We used our introduced figures of merit to evaluate the resistance components of our flow-through CDI cell. We obtained a typical charging profile of our flow-through CDI cell in CV mode at 1 V (see Figure S-3a). We divide the voltage by instant charging current to obtain an ESR as 60.9 Ω. This resistance is much larger than the setup resistance (0.5 Ω) as we estimated from solution and separator properties. This significant resistance difference was also observed by Piotr Dlugolecki et al. in their CDI system.[5] According to our CDI resistance model, we hypothesize that this significant difference is largely due to the contact resistance between current collectors and porous electrodes. To test our hypothesis, we performed EIS to the whole cell (shown in Figure S-3b). The major diameter of the semiellipse in Nyqist plot indicates the contact resistance between the current collector and the porous electrode. The extracted value of this contact resistance is 57.2 Ω, which constitutes 94% of the ESR in our cell. This observation draws attention to investigate the poor electrical contact between the current collector and the porous electrode and supports the hypothesis that contact resistance is the major contributor to effective resistance in CDI cells.

Contact Resistance vs Pressure. We quantified contact resistance between a single interface of HCAM material and a copper plate using our custom four-point measurement platform. Figure 3a shows the results of three repeatable runs on the same sample. The upper three curves represent the contact resistance during application of compressive stress to the HCAM against copper current collector. The lower three curves represent the reverse process as pressure was decreased and the HCAM sample recovered from compression. At the start of the compressions, with minimal pressure between the HCAM sample and copper current collector, the contact resistance was as high as 66 Ω (Figure 3a inset). As pressure increased, contact resistance reduces dramatically, then saturated at approximately 1.5 Ω. These trends suggest that applying a compression pressure to porous electrode and current collector can efficaciously reduce the interfacial contact resistance. We present a qualitative hypothesis for this phenomenon in Figure 3b. The compression force deforms the surface of porous electrode and creates additional microscopic contact regions leading to increased area between electrode and current collector. As pressure increases, the contact area saturates to a certain level. To further characterize the contact between the HCAM and our copper plate, we also performed compression tests to HCAM materials to characterize its elasticity (c.f. Figure S-6). These elasticity tests suggest that, for the pressure range we selected for our compression tests of Figure 3a, our experiments are within the elastic response region for the HCAM. Another indicator that the HCAM was deformed elastically was the resistance values measured during release. The contact resistance half-cycles clearly show hysteresis, but the entire cycle is quite repeatable. That is, the cell repeatedly recovers to its original state, suggesting that the HCAM sample was not crushed or damaged during compression. We also performed EIS measurements on the entire CDI cell as a function of applied pressure. These experiments were conducted with 2 M NaCl solution with 10 mV sinusoidal perturbation voltage. Figure 4b shows Nyquist plots of EIS responses at various pressure conditions. As pressure increased from less than 1 to 30 kPa, the dominant semiellipse of the Nyquist plot shrinks.

DOI: 10.1021/acs.est.5b02542
Environ. Sci. Technol. XXXX, XXX, XXX–XXX

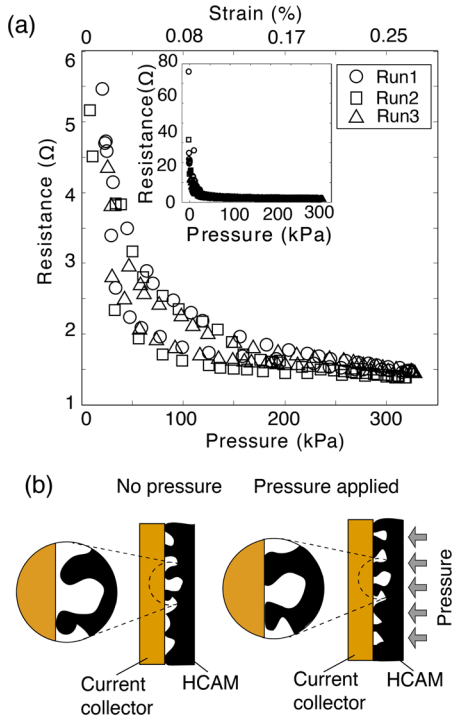

Figure 3. (a) Four-point measurement of contact resistance as a function of varying compressive stress/pressure. The main part is cut off at 6 Ω in order to show the trends of contact resistance. The upper three curves are contact resistance during compression; the lower three lines are contact resistance when releasing pressure. The inset shows the full scale of the measured data. (b) Illustration of the hypothesized mechanism of reducing contact resistance by pressure. Compression deforms microscopic structures on the surface of HCAM sample and creates gradually increasing microscopic electrical contact points between electrode and current collector, and hence the contact resistance decreases.

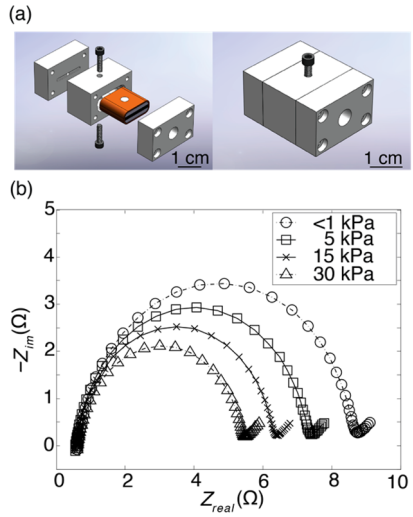

Figure 4. (a) Schematic of full, two-electrode flow-through CDI with compression controllable by two screws in the assembly. The electrode assembly consists of two 2 × 2 × 0.1 cm^3 HCAM pieces, a 25 μm thick porous dielectric separator, and two 2 × 2 × 0.25 cm^3 titanium current collectors. Two screws were used to apply pressure to the electrode assembly. (b) Nyquist plot of flow-through CDI cell under four pressure states. These EIS tests were performed with 2 M NaCl electrolyte. The semiellipse shrunk as applied pressure increased. The value of contact resistance extracted from EIS data reduced from 8.8 Ω to 5.5 Ω as pressure increased from <1 to 30 kPa.

We extracted the numbers of contact resistance and interfacial capacitance from these EIS data using the equivalent circuit of Figure 1b, and summarized the results in Table S-1. The area-normalized values of the extracted interfacial capacitance in our experiments are close to the reported double-layer capacitance of a metallic substrate interfacing with electrolyte.[33] This is further evidence that the semiellipse in Nyquist plot is associated with contact resistance and the parallel interfacial capacitance associated with the interface between the porous electrodes and current collectors. From the extracted numbers, the contact resistance, which is associated with the major diameter of the semiellipse, decreased from 8.8 to 5.5 Ω, nearly 40% reduction. At the same time, the interfacial capacitance was reduced by 7.7% from 22.0 μF to 20.3 μF. The capacitance did not change substantially, but appeared to trend downward with increased pressure. These trends suggest that contact area was created at the expense of reducing the capacitive surface, and that the sum of the microscopic electrical contact area and interfacial capacitance surface area was not constant. Therefore, these data again support the view that applying pressure to press porous electrodes against current collectors is an effective way to reduce contact resistance.

We note that the semiellipse of the EIS measurements and our attribution of this feature to contact resistance is consistent with similar phenomena which have been observed in related fields, including lithium-ion batteries,[31] supercapacitors,[14−16,19] and electroceramic systems.[34] Lei et al. reported the reduction of contact resistance in porous carbon/Al electrical double layer supercapacitors by putting weights on the body of the devices.[14] Dsoke et al. showed that the contact resistance between current collector and composite carbon electrode in supercapacitors could be improved by properly regulating processing parameters, such as temperature and pressure.[15] Hwang et al. demonstrated that mechanical loading reduced the contact impedance of gold electrodes on nanophase cerium dioxide in electroceramic system.[34] We note these non-CDI studies all reported only qualitative EIS data. Also, their systems of interest were describable by different circuit elements and/or by limiting factors different than our CDI system. As far as we know, our work is the first study to quantitatively investigate contact resistance in CDI systems.

Proposed Contact Configuration. We investigated and here propose an alternative contact configuration for contact between a porous electrode and a current collector. We used high conductivity silver epoxy (CW2400, CircuitWorks, Waukegan, IL) to create a spot contact between the porous electrode and copper wire along the thin edge of HCAM sample (Figure 5a). This thin edge connection (versus connection at the face) is convenient for stacks of electrodes and separators and is also more relevant to flow-through CDI cell architectures (e.g., a silver epoxy contact on the large flat face would block liquid flow normal to the large face of the porous electrodes). By infiltrating silver epoxy into a small region of the porous electrode, we created an intimate electrical contact between the HCAM substrate and current collector. Figure 5b qualitatively visualizes the principle behind this reduction of total cell resistance by employing this new contacting configuration. Silver epoxy fills into the microscopic voids between porous electrode and current collector; greatly increase contact area to the HCAM.

In Figure 5c, we show an example quantification of the effect of this contact method. The plot shows two comparative EIS

DOI: 10.1021/acs.est.5b02542
Environ. Sci. Technol. XXXX, XXX, XXX−XXX

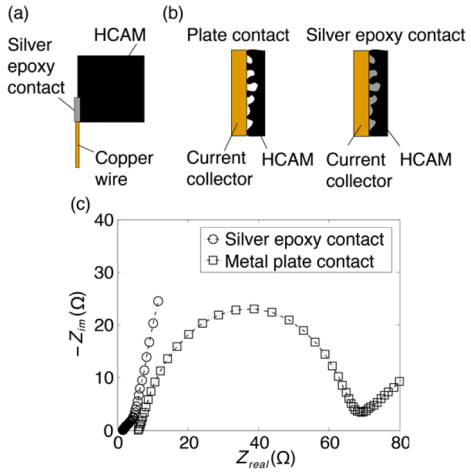

Figure 5. (a) Schematic of silver epoxy point contact on the edge of HCAM sample. (b) Illustration of mechanism of silver epoxy contact. Silver epoxy infiltrating the microscopic air voids within the porous material and between the material and the current collector, thereby reducing contact resistance and eliminating interfacial capacitance. (c) Comparison of Nyquist plots of two electrical contact configuration with 100 mM NaCl: metal plate contact and silver epoxy contact.

experiments of assembled EIS cells performed with 100 mM NaCl solution, to simulate the desalination of brackish water.[1] The semiellipse was completely eliminated from the Nyquist plot, showing the significant reduction of interfacial contact resistance. From the CV/CC charging/discharging cycle data (Table 2), we extracted that the contact resistance reduced to 7.5 Ω using silver epoxy contact, compared to 63 Ω when using titanium plate contact. In addition, the resistance value of the first intersection point with the real axis, namely the setup resistance, was also reduced from 5.9 to 1.5 Ω (a 4-fold reduction). We hypothesize that we can further reduce series resistance in CDI cells by using multiple-spot silver epoxy contacts on the same edge of the electrode. We note here the difference of measured setup resistances of these two contact configurations was due to different wirings. The measured 5.9 Ω of the plate contact configuration (shown in Figure 4a) included the additional resistance from screws and the contact resistance between screws and current collectors, whereas the silver epoxy contact configuration only included setup resistance and silver epoxy resistance. It is worth noting that a directly exposed silver epoxy connection may dissolve or corrode during CDI operation. However, we did not observe noticeable degradation of performance of silver epoxy contact in our system within 4 months of operation. One way to address the corrosion problem is to cover the solver epoxy contact with one or more protection layers, such as epoxy resin (as has been done in other electrochemical systems[35,36]) or silicone.

We note that, given minimal resistance contacts, the resistivity of HCAM samples may become a limiting factor for resistance minimization. For example, contact at the thin edge of an electrode forces electrical current to flow in-plane through small cross-section of the porous electrode. A recent study on 3D bulk nanographene suggests that the resistivity of graphitic carbon materials varies as a function of applied voltages, due to the electrochemically induced accumulation or depletion of charge carriers in combination with a large variation in the carrier mobility.[37] Since HCAMs have high graphitic content, we expect that HCAM may exhibit similar properties. Future

Table 2. Review of Cell Resistance Figures of Merit from Published CDI Studies

first author/ publication year	cell stack no. (N)	area of electrode per cell (A) [cm^2]	thickness of electrode [μm]	salt solution conductivity [mS/cm]	operation mode (CV or CC)	estimated R_s[Ω]	estimated contact resistance R_{ct}[b] [Ω]	estimated ionic resistance R_i[Ω]	area-normalized contact resistance $R_{ct}AN$ [Ω · cm^2]	charging ANESR $(R_s + R_{ct})AN$ [Ω · cm^2]	discharging ANESR $(R_s + R_{ct})AN$ [Ω · cm^2]	area-normalized operational nominal resistance (ANONR) $(R_s + R_{ct} + 1/2R_i)AN$[a] [Ω · cm^2]
Farmer/1996[38]	192	47.1	127	1.0	CV	0.007	0.05	0.013	452	515	605	571
Wang/2006[39]	1	55.7	250	0.19	CV	9.6	25.4	20.3	1415	1950	4179[c]	2517
Kim/2010[40]	1	99.2	330	0.42	CV	0.6	6.9	6.4	687	744	149[c]	1059
Porada/2012[41]	8	33.8	270	0.55	CV	0.3	4.8	1.5	1290	1370	1201	1569
Zhao/2012[4]	8	33.8	362	2.16	CV, CC	0.1	0.6	0.54	161	189	135	263
Suss/2012[42]	1	4.0	1000	10.7	CV	0.5	29.5	20.4	118	120		160
García-Quismondo/2013[9]	8	318	3000	1.7	CC	0.05	0.3	0.6	638	763	560	1535
our cell	1	4.0	1000	10.7	CC, CV	0.5	7.5	20.4	30	32.0		72.8

[a]To estimate operational nominal resistance, we used typically reported tortuosity and porosity numbers for activated carbon and carbon aerogel materials: $\tau_e = 3.5$;[43,44] $\psi_e = 0.8$. [b]Contact resistance is estimated by subtracting estimated R_s from measured charging ESR (R_s+ R_{ct}). [c]Charging resistance and discharging resistances show a significance difference, and this may be due to incomplete charging or discharging.

DOI: 10.1021/acs.est.5b02542
Environ. Sci. Technol. XXXX, XXX, XXX−XXX

work on resistivity change induced by charge accumulation under operational conditions is needed to further characterize the total resistance in CDI systems. Overall, intimate electrical contact (e.g., using the silver epoxy method described here) between a CDI porous electrode and a current collector demonstrates significant improvement regarding minimization of total series resistance of CDI systems.

Review of Reported CDI Cell Resistances. To extend our observations and conclusions to other CDI systems, we have reviewed published reports of CDI cells, and reported resistance values strongly imply that series resistances is a key issue for CDI systems. From the publications that we reviewed, we can easily extract ESR ($R_s + R_{ct}$) and ANESR ($R_s + R_{ct}$)NA from CV mode or CC mode charging/discharging profiles and cell geometries as we described, and estimate resistance R_s and R_i using reported properties of salt solutions, separators, and electrodes (see SI section S-2). Subtracting the calculated R_s value from reported ESR, we obtain an estimate of the missing resistance. In our cell, according to our model and studies on contact resistance, we have demonstrated that this missing resistance is due to the poor electrical contact between current collector and porous electrodes. For other CDI cells reported in the literature, we hypothesize that this missing resistance is also predominantly contact resistance between the current collector and the porous electrode. We here review several instructive examples. Zhao et al. demonstrated a membrane capacitive deionization (MCDI) cell with CC operational mode.[4,10] The reported ESR of their prototype cell is 0.7 Ω as a stack of eight individual cells (5.6 Ω per cell) with 20 mM NaCl solution. However, we estimate that the sum of the ionic resistance in separator, wires and membranes is only about 0.08 Ω as a stack (0.6 Ω per cell), constituting only 11% of reported entire cell resistance. In other words, nearly 90% of the resistance may be contact resistance. García-Quismondo et al. demonstrated a method to isolate the effects between charging and discharging cycles with their flow-between CDI reactor.[9] Their cell had an ESR of 0.3 Ω as a stack (2.4 Ω per cell) in CC operation mode, whereas our calculated estimate of their setup resistance is only 0.05 Ω as a stack (0.4 Ω per cell). And so 83% of the ESR was possibly from the electrical contact. We summarized the reported resistance of each published CDI cell that we reviewed, and the associated resistance estimates in Table 2. These reported values of cell resistance support strongly the hypothesis that contact resistance nearly always dominates cell resistance for reported devices.

In conclusion, we here report our efforts to characterize resistance components in capacitive deionization (CDI) systems. We propose two area-normalized standards as a merit matrix to evaluate resistances across CDI devices: area-normalized equivalent series resistance and area-normalized operational nominal resistance. We found that the contact resistance between current collector and porous electrode was the major contributor of series resistance in our CDI cell, and we think that it is also the main resistance component in published CDI cells we reviewed. We further propose and demonstrate two methods to minimize contact resistance. The first is application of sufficient pressure to press porous electrodes against current collectors. The second is an alternative and convenient electrical contact configuration: providing intimate contact between the porous electrode and current collector. By implementing our methods, the energy cost of CDI could be reduced by up to 88% and makes CDI the most energy efficient desalination method for low-salinity waters. On the basis of the study by Zhao et al., if the contact resistance could be eliminated, the energy cost of CDI would be lower than RO by as much as a factor of 4 to 20 for the salt concentration ranging from 1.2 g/L to 4 g/L.[3]

Lastly, we note that, surprisingly, characteristic cell resistances are rarely reported in published studies of CDI cells. Energy consumption is a key figure of merit for the performance of CDI, and resistance is an important factor. We suggest that reporting device resistance should become a standard metric for CDI publications, just as removal capacity and removal rate have already become, and we recommend use of our proposed two area-normalized resistance metrics.

■ ASSOCIATED CONTENT

Supporting Information

The Supporting Information is available free of charge on the ACS Publications website at DOI: 10.1021/acs.est.5b02542.

Information and figures further describing calculation and estimation of resistances in capacitive deionization (CDI) cells; LTSpice simulations of time-dependent current or voltage responses of CDI systems based on our model; and measured mechanical properties of hierarchical carbon aerogel monoliths (HCAMs) (PDF)

■ AUTHOR INFORMATION

Corresponding Authors

*Tel.: 650-723-5689; fax: 650-723-7657; e-mail: juan.santiago@stanford.edu (J.G.S.).

*Tel.: 925-423-9128; e-mail: stadermann2@llnl.gov (M.S.).

Author Contributions

The manuscript was written through contributions of all authors. All authors have given approval to the final version of the manuscript.

Notes

The authors declare no competing financial interest.

■ ACKNOWLEDGMENTS

Y.Q. would like to thank the Lawrence Scholar program. Work at LLNL was performed under the auspices of the US DOE by LLNL under Contract DE-AC52-07NA27344.

■ REFERENCES

(1) Porada, S.; Zhao, R.; van der Wal, A.; Presser, V.; Biesheuvel, P. M. Review on the science and technology of water desalination by capacitive deionization. *Prog. Mater. Sci.* **2013**, *58* (8), 1388−1442.

(2) Anderson, M. A.; Cudero, A. L.; Palma, J. Capacitive deionization as an electrochemical means of saving energy and delivering clean water. Comparison to present desalination practices: Will it compete? *Electrochim. Acta* **2010**, *55* (12), 3845−3856.

(3) Zhao, R.; Porada, S.; Biesheuvel, P. M.; van der Wal, A. Energy consumption in membrane capacitive deionization for different water recoveries and flow rates, and comparison with reverse osmosis. *Desalination* **2013**, *330*, 35−41.

(4) Zhao, R.; Biesheuvel, P. M.; van der Wal, A. Energy consumption and constant current operation in membrane capacitive deionization. *Energy Environ. Sci.* **2012**, *5* (11), 9520−9527.

(5) Dlugolecki, P.; van der Wal, A. Energy recovery in membrane capacitive deionization. *Environ. Sci. Technol.* **2013**, *47* (9), 4904−4910.

(6) Demirer, O. N.; Naylor, R. M.; Rios Perez, C. A.; Wilkes, E.; Hidrovo, C. Energetic performance optimization of a capacitive deionization system operating with transient cycles and brackish water. *Desalination* **2013**, *314*, 130−138.

(7) Garcia-Quismondo, E.; Santos, C.; Lado, J.; Palma, J.; Anderson, M. A. Optimizing the energy efficiency of capacitive deionization

DOI: 10.1021/acs.est.5b02542
Environ. Sci. Technol. XXXX, XXX, XXX−XXX

reactors working under real-world conditions. *Environ. Sci. Technol.* **2013**, *47* (20), 11866−11872.
(8) Kim, T.; Dykstra, J. E.; Porada, S.; van der Wal, A.; Yoon, J.; Biesheuvel, P. M. Enhanced charge efficiency and reduced energy use in capacitive deionization by increasing the discharge voltage. *J. Colloid Interface Sci.* **2015**, *446*, 317−26.
(9) Garcia-Quismondo, E.; Gomez, R.; Vaquero, F.; Cudero, A. L.; Palma, J.; Anderson, M. New testing procedures of a capacitive deionization reactor. *Phys. Chem. Chem. Phys.* **2013**, *15* (20), 7648−7656.
(10) Zhao, R.; Satpradit, O.; Rijnaarts, H. H.; Biesheuvel, P. M.; van der Wal, A. Optimization of salt adsorption rate in membrane capacitive deionization. *Water Res.* **2013**, *47* (5), 1941−1952.
(11) Kang, J.; Kim, T.; Jo, K.; Yoon, J. Comparison of salt adsorption capacity and energy consumption between constant current and constant voltage operation in capacitive deionization. *Desalination* **2014**, *352*, 52−57.
(12) Pandolfo, A. G.; Wilson, G. J.; Huynh, T. D.; Hollenkamp, A. F. The influence of conductive additives and inter-particle voids in carbon EDLC electrodes. *Fuel Cells* **2010**, *10* (5), 856−864.
(13) Pell, W. G.; Conway, B. E.; Marincic, N. Analysis of non-uniform charge/discharge and rate effects in porous carbon capacitors containing sub-optimal electrolyte concentrations. *J. Electroanal. Chem.* **2000**, *491* (1−2), 9−21.
(14) Lei, C.; Markoulidis, F.; Ashitaka, Z.; Lekakou, C. Reduction of porous carbon/Al contact resistance for an electric double-layer capacitor (EDLC). *Electrochim. Acta* **2013**, *92*, 183−187.
(15) Dsoke, S.; Tian, X.; Täubert, C.; Schlüter, S.; Wohlfahrt-Mehrens, M. Strategies to reduce the resistance sources on Electrochemical Double Layer Capacitor electrodes. *J. Power Sources* **2013**, *238*, 422−429.
(16) Wu, H.-C.; Lin, Y.-P.; Lee, E.; Lin, W.-T.; Hu, J.-K.; Chen, H.-C.; Wu, N.-L. High-performance carbon-based supercapacitors using Al current-collector with conformal carbon coating. *Mater. Chem. Phys.* **2009**, *117* (1), 294−300.
(17) Pasquier, A. D.; Plitz, I.; Gural, J.; Menocal, S.; Amatucci, G. Characteristics and performance of 500 F asymmetric hybrid advanced supercapacitor prototypes. *J. Power Sources* **2003**, *113*, 62−71.
(18) Taberna, P. L.; Simon, P.; Fauvarque, J. F. Electrochemical characteristics and impedance spectroscopy studies of carbon-carbon supercapacitors. *J. Electrochem. Soc.* **2003**, *150* (3), A292−A300.
(19) Portet, C.; Taberna, P. L.; Simon, P.; Laberty-Robert, C. Modification of Al current collector surface by sol−gel deposit for carbon−carbon supercapacitor applications. *Electrochim. Acta* **2004**, *49* (6), 905−912.
(20) Momma, T.; Liu, X.; Osaka, T.; Ushio, Y.; Sawada, Y. Electrochemical modification of active carbon fiber electrode and its application to double-layer capacitor. *J. Power Sources* **1996**, *60* (2), 249−253.
(21) Horiba, T.; Hironaka, K.; Matsumura, T.; Kai, T.; Koseki, M.; Muranaka, Y. Manganese-based lithium batteries for hybrid electric vehicle applications. *J. Power Sources* **2003**, *119−121*, 893−896.
(22) Nugrahenny, A. T. U.; Kim, J.; Lim, S.; Jung, D.-H. Development of high performance cell structor for capacitive deionization using membrane polymer-coated electrode. In *The 6th Conference of Indonesian Students Association in Korea*, Daejeon.
(23) Limpt, B. v. Performance relations in capacitive deionization systems. Ph.D. Dissertation, Wageningen University: Wageningen, Netherlands, 2010.
(24) Baumann, T. F.; Worsley, M. A.; Han, T. Y.-J.; Satcher, J. H. High surface area carbon aerogel monoliths with hierarchical porosity. *J. Non-Cryst. Solids* **2008**, *354* (29), 3513−3515.
(25) Suss, M. E.; Baumann, T. F.; Worsley, M. A.; Rose, K. A.; Jaramillo, T. F.; Stadermann, M.; Santiago, J. G. Impedance-based study of capacitive porous carbon electrodes with hierarchical and bimodal porosity. *J. Power Sources* **2013**, *241*, 266−273.
(26) Suss, M. E.; Baumann, T. F.; Bourcier, W. L.; Spadaccini, C. M.; Rose, K. A.; Santiago, J. G.; Stadermann, M. Capacitive desalination with flow-through electrodes. *Energy Environ. Sci.* **2012**, *5* (11), 9511−9519.
(27) Levie, R. d. On porous electrodes in electrolyte solutions IV. *Electrochim. Acta* **1964**, *9* (9), 1231−1245.
(28) Brug, G. J.; van den Eeden, A. L. G.; Sluyters-rehbach, M.; Sluyters, J. H. The analysis of electrode impedance complicated by the presence of a constant phase element. *J. Electroanal. Chem. Interfacial Electrochem.* **1984**, *176*, 275−295.
(29) Barsoukov, E.; Macdonald, J. R. *Impedance Spectroscopy: Theory, Experiment, and Applications*, 2nd ed.; Wiley: Hoboken, NJ, 2005.
(30) Hsu, C. H.; Mansfeld, F. Technical note: concerning the conversion of the constant phase element parameter Y_0 into a capacitance. *Corrosion* **2001**, *57* (9), 747−748.
(31) Gaberscek, M.; Moskon, J.; Erjavec, B.; Dominko, R.; Jamnik, J. The Importance of Interphase Contacts in Li Ion Electrodes: The Meaning of the High-Frequency Impedance Arc. *Electrochem. Solid-State Lett.* **2008**, *11* (10), A170.
(32) Yao, S.; Santiago, J. G. Porous glass electroosmotic pumps: theory. *J. Colloid Interface Sci.* **2003**, *268*, 133−142.
(33) Norlin, A.; Pan, J.; Leygraf, C. Investigation of interfacial capacitance of Pt, Ti and TiN coated electrodes by electrochemical impedance spectroscopy. *Biomol. Eng.* **2002**, *19*, 67−71.
(34) Hwang, J.-H.; Kirkpatrick, K. S.; Mason, T. O.; Garboczi, E. J. Experimental limitation in impedance spectroscopy: Part IV. Electrode contact effects. *Solid State Ionics* **1997**, *98*, 93−104.
(35) Al-Kayiem, H. H.; Brebbia, C. A.; Zubir, S. S. *Energy and Sustainability V.*; WIT Press: Southampton, UK, 2015.
(36) Bartlett, P. N.; Perdjon-Abel, M.; Cook, D.; Reid, G.; Levason, W.; Cheng, F.; Zhang, W.; George, M. W.; Ke, J.; Beanland, R.; Sloan, J. The Electrodeposition of Silver from Supercritical Carbon Dioxide/Acetonitrile. *ChemElectroChem* **2014**, *1* (1), 187−194.
(37) Dasgupta, S.; Wang, D.; Kübel, C.; Hahn, H.; Baumann, T. F.; Biener, J. Dynamic control over electronic transport in 3D bulk nanographene via interfacial charging. *Adv. Funct. Mater.* **2014**, *24* (23), 3494−3500.
(38) Farmer, J. C.; Fix, D. V.; Mack, G. V.; Pekala, R. W.; Poco, J. F. Capacitive deionization of NaCI and $NaNO_3$ solutions with carbon aerogel electrodes. *J. Electrochem. Soc.* **1996**, *143* (1), 159−169.
(39) Wang, X. Z.; Li, M. G.; Chen, Y. W.; Cheng, R. M.; Huang, S. M.; Pan, L. K.; Sun, Z. Electrosorption of NaCl solutions with carbon nanotubes and nanofibers composite film electrodes. *Electrochem. Solid-State Lett.* **2006**, *9* (9), E23−E26.
(40) Kim, Y.-J.; Choi, J.-H. Enhanced desalination efficiency in capacitive deionization with an ion-selective membrane. *Sep. Purif. Technol.* **2010**, *71* (1), 70−75.
(41) Porada, S.; Weinstein, L.; Dash, R.; van der Wal, A.; Bryjak, M.; Gogotsi, Y.; Biesheuvel, P. M. Water desalination using capacitive deionization with microporous carbon electrodes. *ACS Appl. Mater. Interfaces* **2012**, *4* (3), 1194−1199.
(42) Suss, M. Capacitive water desalination with hierarchical porous electrodes. Ph.D. Dissertation, Stanford University: Stanford, CA, 2013.
(43) Jayne, D.; Zhang, Y.; Haji, S.; Erkey, C. Dynamics of removal of organosulfur compounds from diesel by adsorption on carbon aerogels for fuel cell applications. *Int. J. Hydrogen Energy* **2005**, *30*, 1287−1293.
(44) Leyva-Ramos, R.; Geankoplis, C. J. Diffusion in liquid-filled pores of activated carbon. I. Pore volume diffusion. *Can. J. Chem. Eng.* **1994**, *72*, 262−271.

DOI: 10.1021/acs.est.5b02542
Environ. Sci. Technol. XXXX, XXX, XXX−XXX